Journal of Biomedical Optics

BiomedicalOptics.SPIEDigitalLibrary.org

Distinguishing tracheal and esophageal tissues with hyperspectral imaging and fiber-optic sensing

Corinne D. Nawn
Brian E. Souhan
Robert Carter, III
Caitlin Kneapler
Nicholas Fell
Jing Yong Ye

SPIE.

Corinne D. Nawn, Brian E. Souhan, Robert Carter, , IIICaitlin Kneapler, Nicholas Fell, Jing Yong Ye, "Distinguishing tracheal and esophageal tissues with hyperspectral imaging and fiber-optic sensing," *J. Biomed. Opt.* **21**(11), 117004 (2016), doi: 10.1117/1.JBO.21.11.117004.

Distinguishing tracheal and esophageal tissues with hyperspectral imaging and fiber-optic sensing

Corinne D. Nawn,[a,b,c,d,*] Brian E. Souhan,[e] Robert Carter III,[a,d] Caitlin Kneapler,[e] Nicholas Fell,[e] and Jing Yong Ye[c,d]
[a]United States Army Institute of Surgical Research, 3698 Chambers Pass, Fort Sam Houston, Texas 78234, United States
[b]Oak Ridge Institute for Science and Education, 4692 Millennium Drive, Suite 101, Belcamp, Maryland 21017, United States
[c]University of Texas at San Antonio, One UTSA Circle, San Antonio, Texas 78249, United States
[d]University of Texas Health Science Center at San Antonio, 7703 Floyd Curl Drive, Mail Code 7736, San Antonio, Texas 78229, United States
[e]United States Military Academy, 606 Thayer Road, West Point, New York 10996, United States

Abstract. During emergency medical situations, where the patient has an obstructed airway or necessitates respiratory support, endotracheal intubation (ETI) is the medical technique of placing a tube into the trachea in order to facilitate adequate ventilation of the lungs. Complications during ETI, such as repeated attempts, failed intubation, or accidental intubation of the esophagus, can lead to severe consequences or ultimately death. Consequently, a need exists for a feedback mechanism to aid providers in performing successful ETI. Our study examined the spectral reflectance properties of the tracheal and esophageal tissue to determine whether a unique spectral profile exists for either tissue for the purpose of detection. The study began by using a hyperspectral camera to image excised pig tissue samples exposed to white and UV light in order to capture the spectral reflectance properties with high fidelity. After identifying a unique spectral characteristic of the trachea that significantly differed from esophageal tissue, a follow-up investigation used a fiber optic probe to confirm the detectability and consistency of the different reflectance characteristics in a pig model. Our results characterize the unique and consistent spectral reflectance characteristic of tracheal tissue, thereby providing foundational support for exploiting spectral properties to detect the trachea during medical procedures. [DOI: 10.1117/1.JBO.21.11.117004]

Keywords: trachea; esophagus; intubation; fiber optic; hyperspectral camera; spectral characterization.

Paper 160471PR received Jul. 6, 2016; accepted for publication Nov. 1, 2016; published online Nov. 23, 2016.

1 Introduction

Endotracheal intubation (ETI) is a frequent life-saving medical procedure, often performed in a prehospital or emergency medicine environment when a patient cannot sufficiently breathe of their own accord. Common medical emergencies, such as cardiac arrest or trauma, often necessitate paramedics or nurses to perform ETI in a chaotic prehospital setting. According to the 2010 Advanced Cardiac Life Support guidelines, a confirmatory procedure should be performed after every ETI to ensure tracheal placement.[1] Failed intubations can lead to death through hypoxemia or unrecognized intubation of the esophagus. Even successful intubations, if delayed or performed poorly, can still encounter major adverse events, such as cardiac arrest, hypotension, hypoxemia, or asphyxiation due to patient aspiration.[2–4] Furthermore, multiple attempts at ETI have been shown to significantly increase the probability of these adverse events, jumping from 14.2% on the first attempt success to 47.2% on the second attempt, to 63.6% chance of adverse events if three attempts were made.[3] In addition to the number of attempts, the time to intubation also adds risk to patient outcomes with longer intubation times leading to extended oxygen deprivation, which has been associated with worse long-term outcomes for traumatic brain injury patients.[5]

Currently, the "gold standard" of confirmation of tracheal tube placement is direct visualization of the endotracheal (ET) tube passing through the vocal chords and observation of the chest rising and falling with ventilation. However, visual depth into the patient's upper airway can often be severely limited due to their clinical condition, such as maxillofacial trauma or swollen features, or due to the geometry of their innate anatomical characteristics, such as prominent teeth or short necks. These challenges, generally categorized as a "difficult airway," have been documented to occur in the prehospital environment as much as 50% of the time and pose problems for standard intubation and visual confirmation techniques.[6,7] Presently, end-tidal carbon dioxide monitoring ($ETCO_2$) exists as a nonvisual method of confirmation for ET placement and can be captured using a few approaches: colorimetry, capnography, or capnometry. The colorimetric approach involves a single-use device with chemical sensitive paper that changes color with the detection of CO_2.[8] When regarded for the prehospital environment, reports have found the colorimetric method subjective and slow as it requires several breathes to allow enough exposure for color differentiation, which is not always sufficiently available during the event of cardiac arrest.[9,10] Studies have also reported false positives when the patient has previously been exposed to mouth-to-mouth resuscitation or if the sensor has been exposed to acidic contents or drugs, such as gastric contents or lidocaine, both of which are common in the prehospital setting.[10,11] Furthermore, colorimetry does not provide continuous patient monitoring to ensure proper tracheal tube

*Address all correspondence to: Corinne D. Nawn, E-mail: nawn.cori@gmail.com

placement once intubated. Displacement of the tracheal tube can result from patient movement, which can easily go undetected amidst the typically chaotic prehospital, ICU, and emergency department environments, thereby leading to the same serious adverse events of failed airway management.[12] Due to these limitations, some guideline documents have formally discouraged the use of the colorimetric approach for prehospital intubation confirmation. On the other hand, capnography involves the monitoring of the waveform measuring instantaneous CO_2 in the expired breath by detecting the change in the relative absorption of infrared light shined through the ET. Correspondingly, capnometry includes the monitoring of the numerical $ETCO_2$ output captured by the capnography. Both capnography and capnometry have been largely correlated with diagnostic benefits as well as ET confirmation.[9–11] Despite its clinical efficacy and suggested benefit, a recent survey of emergency physicians showed only 25% of sites possess continuous $ETCO_2$ monitoring capabilities. This dramatic lack of availability of the technology contrary to its recommendation from professional societies suggests that the instrumentation is too expensive or too much of a hindrance to prehospital care.[13] Additionally, all of the current methods require the provider to stop care to perform the confirmation or they require additional specialized equipment that is not always readily available. In a prehospital or emergency setting, time is critical and providers often cannot afford to stop care to perform or wait for confirmatory procedures.

Consequently, there exists a need for a nonvisual detection mechanism for confirming the ET placement that can rapidly give the user feedback during the procedure. Since different biological tissues possess different properties unique to their form and function, our study endeavored to explore whether the tracheal and esophageal tissues' spectral responses to white and UV light would exhibit a detectible difference. We began by preliminarily investigating the spectra of excised pig tracheal and esophageal tissue using a hyperspectral camera. Based upon our findings from the *ex vivo* studies that tracheal tissue exhibited unique characteristics, we continued *in situ* swine models to investigate the reliability of the characteristic and its relative detectability using fiber optic sensors, a more practical technology for clinical sensing. We hypothesize that by first characterizing the tracheal and esophageal tissue with high resolution *ex vivo*, we could then determine and detect the unique spectral properties of tracheal tissue versus esophageal tissues using fiber optic sensors *in situ* with a pig model.

2 Materials and Methods

Our investigation consisted of two stages: *ex vivo* and *in situ* studies. Our initial exploration aimed to investigate the spectral response of tracheal and esophageal tissue samples, excised from pigs, while our continued experiments endeavored to confirm the initial investigations in pig models with more clinically applicable technologies.

2.1 *Ex Vivo Testing*

Tests exploring the spectral properties of tracheal and esophageal tissue were first conducted at the Photonics Research Center at the United States Military Academy in West Point, New York, using excised porcine tissue samples ordered from Animal Biotech Industries (Danboro, Pennsylvania). Two intact larynx, trachea, and esophagus samples were harvested and shipped overnight in a styrofoam cooler stored over ice. All tests were conducted upon receipt within 30 h of harvesting. Both the trachea and esophagus were dissected from the larynx, separated from each other, and sliced longitudinally to expose the inner tissue lining (lumen). Each tissue sample was then dissected into three horizontal sections to represent the upper, mid, and lower portions of the trachea and esophagus, respectively. Additional slices of the epiglottis and vocal folds were also taken from larynx, the region just above both the separation of the trachea and esophagus. All slices were individually mounted onto cork such that they lay flat for imaging with the hyperspectral camera.

2.2 *Hyperspectral Camera Instrumentation*

Images of the tissue were taken using an OKSI Hyperscan VNIR imager and HyperVision software (Opto-Knowledge Systems, Inc., Torrance, California). The camera consisted of a 696×1314 pixel array and was paired with a 70-mm Apochromat lens yielding an approximate 80-μm spatial resolution. Spectral data were collected in a sweep mode with the resulting data cube yielded one column of spatial data with the full 520 wavelength elements for each CCD exposure, resulting in a total image spectrum from 396 to 1050 nm at each pixel with a 1.25-nm spectral resolution. All samples were illuminated with four white lights (4700 K, D50) and one UV LED (396 nm, Edmund Optics, Barrington, New Jersey) within a fully enclosed blackout box to isolate the camera and sample from external light. The lights were manually positioned to provide uniform illumination with the UV LED positioned to provide maxima illumination at the center of the target.

To obtain a background noise offset, a dark reference spectrum was collected with all the lights off and the camera shutter closed. A white reference spectrum was also collected by imaging a 99% reflectivity standard (5# White Balance Target, #58-610, Edmund Optics, Barrington, New Jersey) exposed to all five lights. The integration time was set to avoid saturation of the white reference. The data collected from each image were then normalized, accounting for both the white and dark spectra of the camera, using the following equation:

$$\text{Reflectance} = \frac{\text{Signal} - \text{Dark}}{\text{White} - \text{Dark}}, \tag{1}$$

where "signal" represents the image data collected from the sample, "dark" represents the calibration image collected with the shutter closed and lights off, and "white" represents the calibration image data collected from a 100% reflectance standard with the lights on after setting the integration time. The data collected were then processed using the Environment for Visualizing Images v4.8 software package (Excelis Visual Information Solutions, Boulder, Colorado).

2.3 *Ex Vivo Data Analysis*

After imaging, the hyperspectral data were processed with the Hypervision software to generate spectral curves for multiple points on each section of the trachea and esophagus along with corresponding color images of the complete imaged section. Each sampled point consisted of a 10×10 pixel square, with each pixel comprising an approximate 81×81 μm^2 of the imaged section. Choosing to analyze the spectra within a 10×10 pixel square helped average out any noise and also resulted in each spectral curve being the average spectral

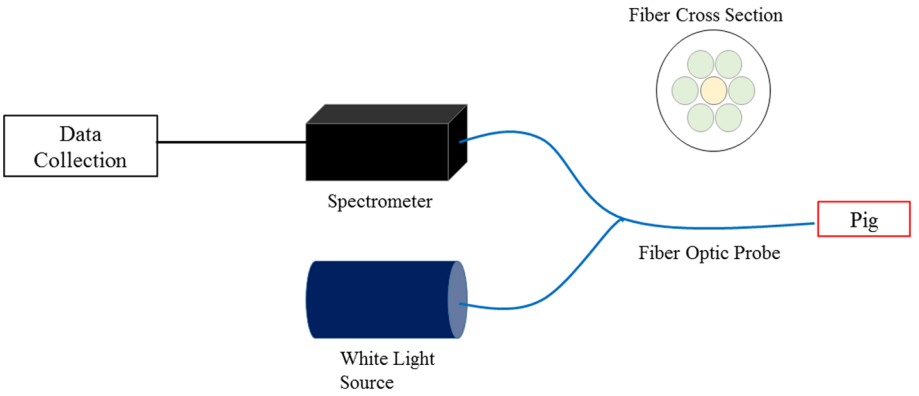

Fig. 1 System block diagram of experimental setup with compact spectrometer and halogen white light source connected to the bifurcated reflection probe with a cross-sectional arrangement of six collecting fibers around one emitting fiber.

reflectance over ~0.65-mm^2 area on the imaged section. From a practical sense, with our future investigations targeting fiber optic and discrete sensors, we felt that analyzing the reflectance spectra with this perspective would more accurately reflect the sensing area of a probe in close proximity of the tissue than by analyzing pixels individually.

2.4 *In Situ Testing*

In situ tests were conducted at the United States Army Institute of Surgical Research in Fort Sam Houston, Texas. Pig models were obtained from a previously approved Institutional Animal Care and Use Committee protocol within the Institute involving a procedure that ended in humane euthanasia and did not compromise the properties of the upper respiratory system. In order to remain as close as practical to *in vivo* representation, spectral data were collected from each pig within 2 min of the euthanasia before any postmortem changes or degradation could affect the local tracheal and esophageal tissue properties.

For *in situ* testing, reflectance spectra were captured using a fiber optic reflection probe connected to a compact spectrometer and a halogen white light source, as shown in Figs. 1 and 2. The fiber optic probe was a 200-μm core, 2-m long bifurcated reflection probe (R200-7-UV-VIS, Ocean Optics, Dunedin, Florida) with a central light emitting fiber with six collection fibers surrounding it to capture the light reflected from the luminal tissue, as diagrammed in Fig. 1 and displayed in Fig. 2.

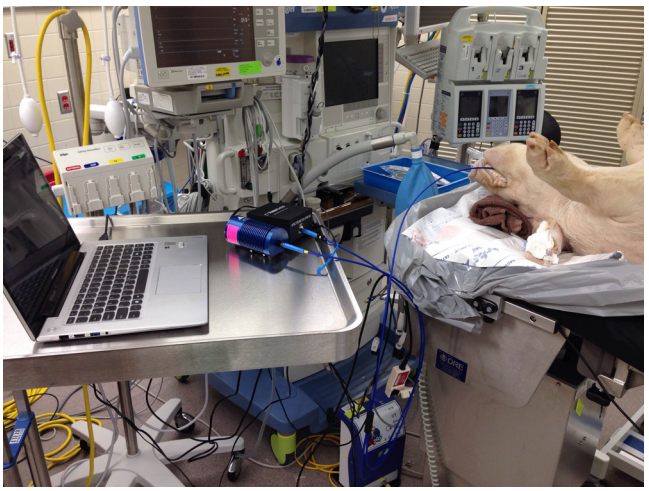

Fig. 2 Fiber optic instrumentation setup, as systematically diagrammed in Fig. 1.

The compact spectrometer was sensitized for 420 to 1070 nm with a 2048 × 14 pixel Hamamatsu S9840 back-thinned CCD (SPM-002-DT, Photon-Control, Vancouver, British Columbia, Canada) and was connected through USB to a laptop with SpecSoft software to display the spectra in real time and capture them for postanalysis. The exposure time was set to 5 ms in order to prevent saturating the detector from the output power of 8.8 mW from the halogen lamp white light source (HL-2000-HP, Ocean Optics). To help mitigate some of the noise, five subsequent exposures were averaged to amount to 25 ms of total exposure time. To account for background interference and the imperfections of the white light source, dark and white reference spectra were collected and stored. The dark spectrum was stored with all ambient lights and the white light source off while the probe was covered with black felt. The white light source was then turned on and the distal end of the probe placed in a white integration sphere (FIOS-1, Ocean Optics) to capture the reference white spectrum. The same reference spectra were loaded before each data collection.

Figure 3 shows the instrumentation of the ET tube in the trachea and the relative placement of the fiber optic probe into the trachea [Fig. 3(a)] and the esophagus [Fig. 3(b)]. The ET tube remained in the trachea from the procedure, and the fiber optic probe was passed through the tube into the tracheal region. The tube was then retracted to expose the distal end to the luminal tissue and the reflectance spectrum was displayed in real-time using SpecSoft and was captured. The probe was repositioned to capture the reflectance profile from six locations within the trachea. After saving the tracheal reflectance spectra, the probe was removed from the ET tube and cleaned with an isopropanol surface disinfectant wipe (CaviWipe™, Metrex Research, LLC, Orange, California). The probe was then inserted into the esophagus and the reflectance spectrum was displayed, captured, and stored at six different locations. The ET tube was left in place to ensure that the probe did not re-enter the trachea.

2.5 *In Situ Data Analysis*

The reflectance, absorbance, and amplitude spectra collected through the SpecSoft Software were stored as text files and imported into MATLAB for spectral analysis. Each pig was numerically identified as 1 through 8, and the respective tracheal and esophageal spectra were organized accordingly. The

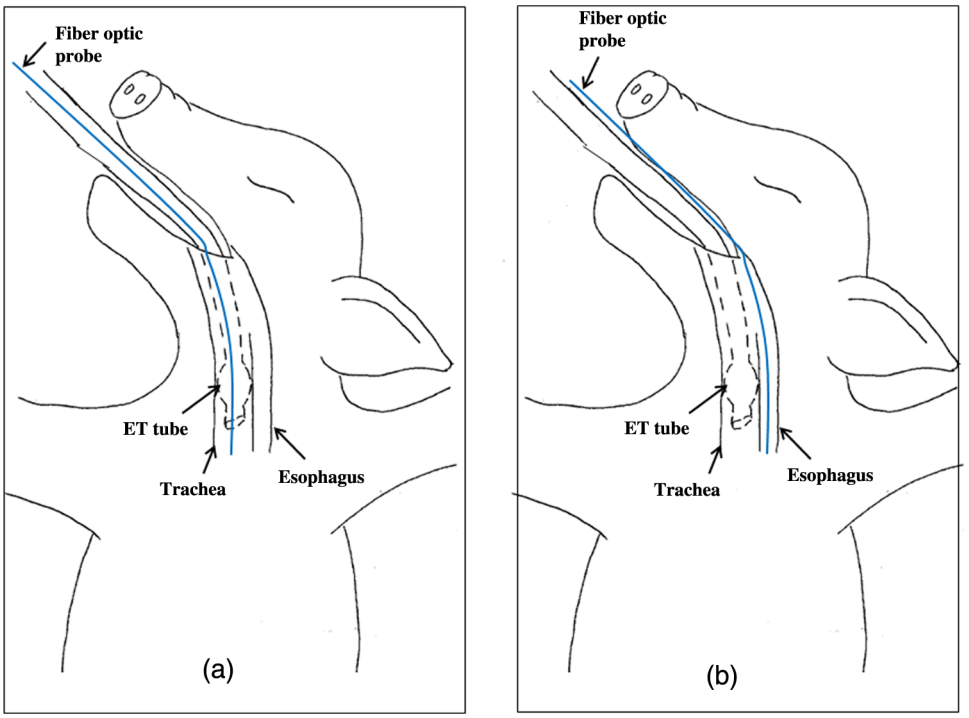

Fig. 3 (a) Fiber optic probe instrumentation when inserted into the tracheal lumen through the endotracheal tube. (b) Fiber optic probe instrumentation for sensing the esophageal lumen by remaining outside and posterior to the ET tube.

tracheal and esophageal spectra were plotted separately and jointly for each pig to isolate as well as compare the unique features. To compare spectra among the pigs, the reflectance spectra for each pig's trachea and esophagus were averaged by summing the value at each data point across the captured profiles and dividing by the number of profiles in order to arrive at one reflectance spectrum representing the trachea and one reflectance spectrum representing the esophagus for each pig. The averaged reflectance spectra were then compared among the pigs by plotting them simultaneously.

To quantitatively characterize and compare the unique features of the spectra, the data were first smoothed by applying a second-order, 15-point framelength Savitsky–Golay filter. Local minima and maxima were then identified in each spectrum, with the mean and standard deviation of the wavelength occurrence of each maximum and minimum determined for each pig. Furthermore, the relative amplitudes, wavelength distances, and slopes were calculated between each maximum and minimum for each spectrum and averaged for one mean per pig. These quantitative characteristics of the minima and maxima were then compared within tissue types and among all pigs for relative similarities as well as between the two tissue types for comparative differences. We chose to assess the relative minima and maxima for the purpose of identifying unique characteristics that could be detected and recognized using discrete components, such as filters, that would be realistic for a prehospital implementation.

3 Results

3.1 *Ex Vivo Results*

Over 200 distinct points were sampled across the two tracheal and esophageal samples. Qualitative examination of the spectral curves from the samples showed no difference among the different sections (upper, middle, and lower) within each respective tissue type; however, the spectral curves of the tracheal tissue compared to the esophageal did show a significant difference in the profiles, as seen in Fig. 4. Figure 4 shows normalized representative samples of the spectral curves found for both the esophagus [Fig. 4(a)] and the trachea [Fig. 4(b)]. The key spectral difference is a distinct peak followed by two local minima seen in the trachea between 530 and 580 nm wherein lies a peak at ~560 nm and the minimum lies near 540 and 577 nm. With the peak qualitatively observed, the data were then normalized to the reflected intensity at the peak (560.9 nm) to both assist in evaluating the peaks qualitatively and determine the strength of the local peak to the relative minima. The insets in Figs. 4(a) and 4(b) show the spectral curve around the peak (535 to 585 nm), clearly showing the distinctive peak seen in the tracheal tissue that is not present in the esophageal tissue.

In order to further characterize the results, the local maxima and minima were compared among upper, middle, and lower sections, between the tissue types and between the two pigs. For the first pig, the location of the maxima and minima was compared between the top and center sections to determine if the location in the trachea had any difference in the spectral characteristics. An independent t-test was conducted on both samples for the two local minima and the local peak. For the top section, the peak was located at 560.9 nm for both sections, resulting in a p-value of 1, showing no statistical difference. The p-values for the two minima of 0.65 and 0.32 also showed no significant difference. Given the lack of significant difference and no known anatomical or physiological differences that would cause the sections to have different spectral responses, the spectral responses from the different points of each section were combined for the trachea and esophagus, respectively.

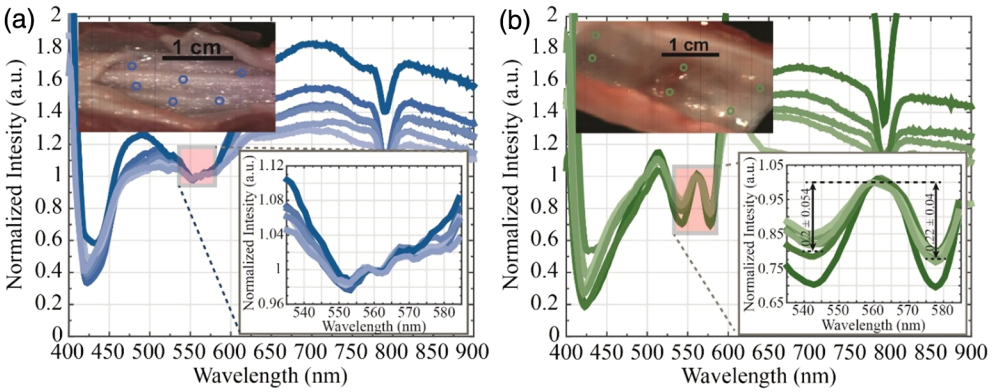

Fig. 4 (a) Reflectance spectra for multiple samples of the esophageal tissue (inset). Reflectance spectra over the area of interest (535 to 585 nm) for the esophageal tissue (image). Colored image taken from the hyperspectral camera with the sample points highlighted by the circles. (b) Reflectance spectra for multiple samples of the tracheal tissue (inset). Reflectance spectra over the area of interest (535 to 585 nm) for the tracheal tissue (image). Colored image taken from the hyperspectral camera with the sample points highlighted by the circles.

For the trachea, the averaging of the spectral curves across the points and sections resulted in a local maximum of 560.9 ± 1.109 nm and local minima locations of 543.242 ± 0.828 nm and 577.917 ± 0.506 for pig one, and 560.377 ± 1.217 nm and local minima locations of 542.398 ± 0.746 nm and 577.082 ± 0.579 for pig two. Analyzing across pigs showed no significant difference in the location of the peaks; but, there was a significant difference in the locations of the minima, with p values of 0.0048 and <0.0001, respectively. Overall, the spectral shape of the "tracheal peak" was the primary characteristic that allowed us to distinguish between the trachea and esophagus subjectively and was enough of a basis to continue research *in situ*.

In addition to just examining the spectral data, we also examined single-band images (each band being 1.25 nm in spectral width) focusing on local minima and maximum seen in the spectral data plot. In order to emphasize the contrast between bands, the same common background darkness was subtracted from all images and the resulting differences scaled to 256 level grayscale. In Figs. 5(a)–5(c), it is seen that the tracheal tissue at the 560.9-nm band in Fig. 5(b) is brighter than the same tissue in Figs. 5(a) and 5(c) at the 541.6- and 577.7-nm bands, as would be expected based on the spectral data. It can also be seen that Fig. 5(e), corresponding to the 560.9-nm band in the esophageal tissue, is less intense than Figs. 5(d) and 5(f), corresponding to the same tissue at the 541.6-nm band and 577.7-nm band, respectively.

3.2 *In Situ Results*

Spectral data were collected on eight pigs, with three to nine spectral captures in both the trachea and esophagus for each pig. In order to collect the data as close to the time of death as possible, the same calibration spectrum was loaded in SpecSoft before each test.

Figures 6(a) and 6(b) show the averaged esophageal and tracheal spectra for all the pigs, with each spectrum representing the average spectral profile for each pig. Initial qualitative

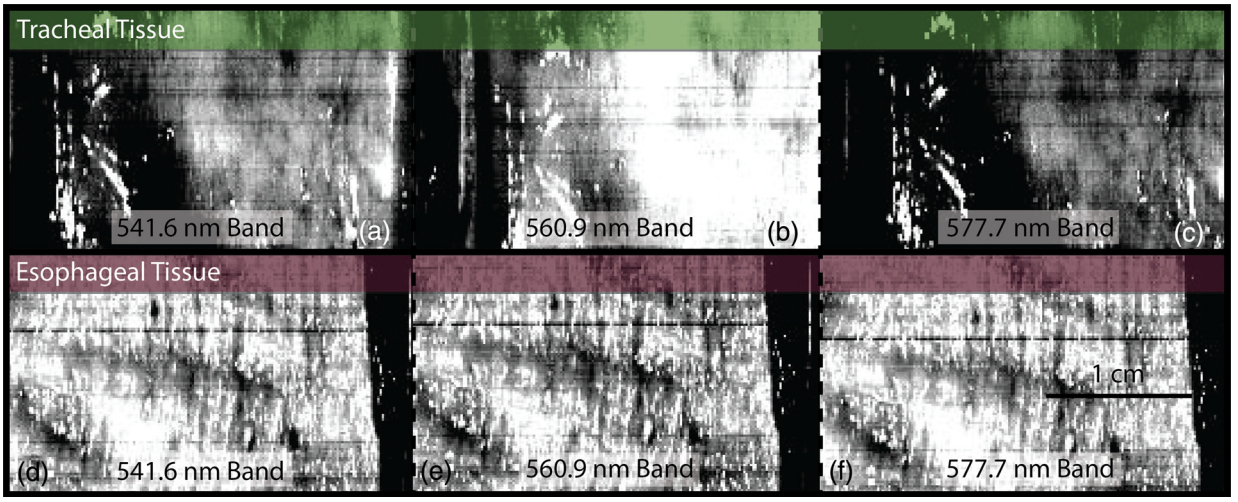

Fig. 5 (a–c) Single-band images of tracheal tissue for wavelength bands centered on (a) 541.6 nm, (b) 560.9 nm, and (c) 577.7 nm, corresponding to the local maxima and local minima seen in Fig. 4(b). (d–f) Single-band images for the esophageal tissue for wavelength bands centered on (d) 541.6 nm, (e) 560.9 nm, and (f) 577.7 nm. The same common background signal was subtracted from each image to highlight the contrast in intensities.

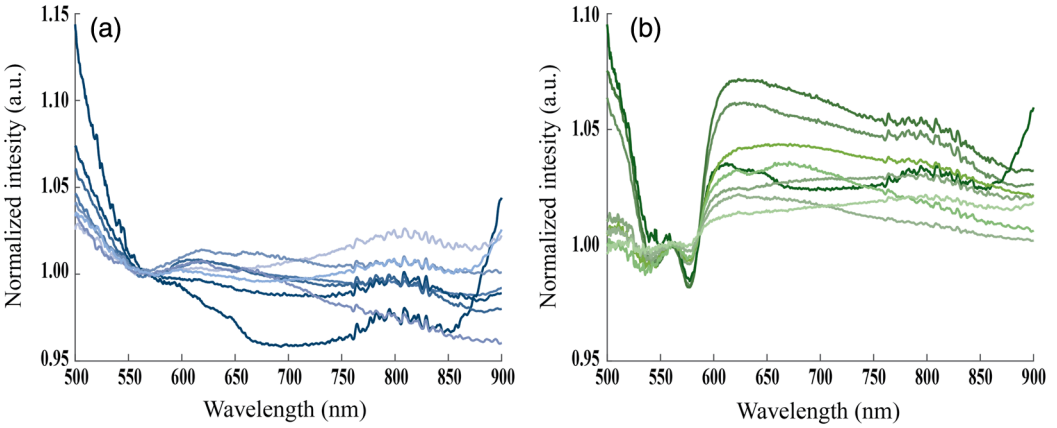

Fig. 6 (a) Normalized esophageal reflectance spectra averaged across all captures for each pig to yield one spectrum per pig. (b) Normalized tracheal reflectance spectra averaged across all captures for each pig to yield one spectrum per pig.

analysis confirmed the existence of the same features as identified by the previous *ex vivo* investigation, with two minima and one maximum within the region of 530 to 580 nm. Conversely, the esophageal spectrum exhibited a gradual negative slope over the same region of interest. The data were then normalized similar to the *ex vivo* results, where the maximum reflectance at the peak occurring around 560 nm was normalized to 1, and then was smoothed using a second-order, 15-point framelength Savitzky–Golay filter.

To further evaluate the relative uniqueness between the spectra, we combined all the individual captures into one joint dataset, including both esophageal ($n = 54$) and tracheal ($n = 57$) spectral data. With each spectrum representing an observation and each wavelength data point representing a variable ($n = 1529$, 450 to 950 nm), we computed the principal components (PCs) of the collective tracheal and esophageal dataset. Figure 7 shows the first two PCs extracted from the combined esophageal and tracheal data plotted alongside the mean spectrum for each of the trachea and esophagus. The individual means of the tracheal and esophageal spectra were calculated by averaging all the tracheal spectra and all of the esophageal spectra (Fig. 6) separately. Since the normalized data from the averaged tissue spectra were normalized, such that the intensity at 560 nm was set to 1, the data were renormalized to set 560 nm to 0 such that it matched up with the PCs.

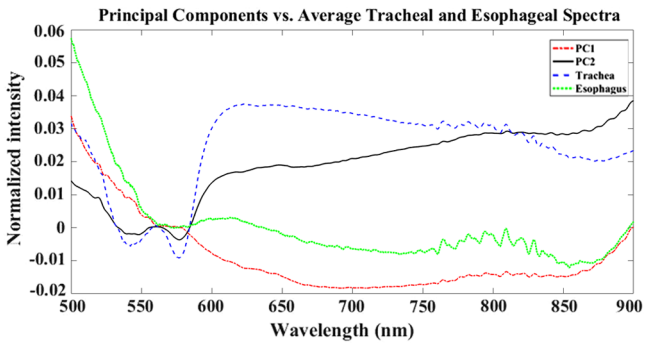

Fig. 7 PC1 and PC2 from the combined tracheal and esophageal data set plotted versus the averaged spectrum from all the tracheal captures (trachea) and all the esophageal captures (esophagus).

The first principal component (PC1) and the esophageal mean spectrum resulted in a positive correlation coefficient of 0.9145 ($p < 0.0001$), whereas the second principal component (PC2) and the tracheal mean spectrum also showed a positive correlation coefficient of 0.6724 ($p < 0.0001$). Conversely, when the esophageal mean was compared with PC2 and the tracheal mean compared with PC1, both yielded significant negative correlation coefficients of −0.5143 and −0.5902, respectively.

As highlighted from observing both the normalized spectra and the PC comparisons, the 530- to 580-nm region still exhibited the most unique characteristic that was not present in the esophageal spectra. To focus in on this region of interest, we identified the maxima and minima, and their wavelength occurrences within the 530 to 580 nm region for both esophageal and tracheal tissue. The wavelength occurrences and amplitudes were subsequently plotted using open circles on top of the spectra plots, as shown in Fig. 8, to superimpose the detected maxima and minima on the spectra. Figures 8(a) and 8(b) show examples of the smoothed spectral data zoomed in on the region of interest with the minima and maxima circled for both the esophagus and trachea, respectively.

For the purpose of clear viewing of the comparative points and individual spectra, the data shown in Fig. 8 were not normalized. As seen from the superimposed results of the maxima and minima detection (Fig. 8), the three points identified on each spectrum represent the detected minima or maxima within the 530- to 580-nm region. Table 1 shows the mean wavelength occurrences and standard deviations for each local minima or maxima for the respective tissue types, termed point 1, point 2, and point 3 corresponding to the first, second, and third points detected within the region. Both the numerical values and the previous spectral graphs highlight that the tracheal tissue exhibited the consistent pattern of two local minima, points 1 and 3, with one local maximum, point 2. On the other hand, the esophageal tissue most often exhibited a pattern of two local maxima, points 1 and 3, with one minimum, point 2. Due to the nature of the gradually decreasing reflectance over the 530- to 580-nm region, 13% of the individual esophageal spectra did not yield a third significant point as the interval only showed one local maximum at the beginning, near 530 nm, and one local minimum at the end of the interval, near 580 nm.

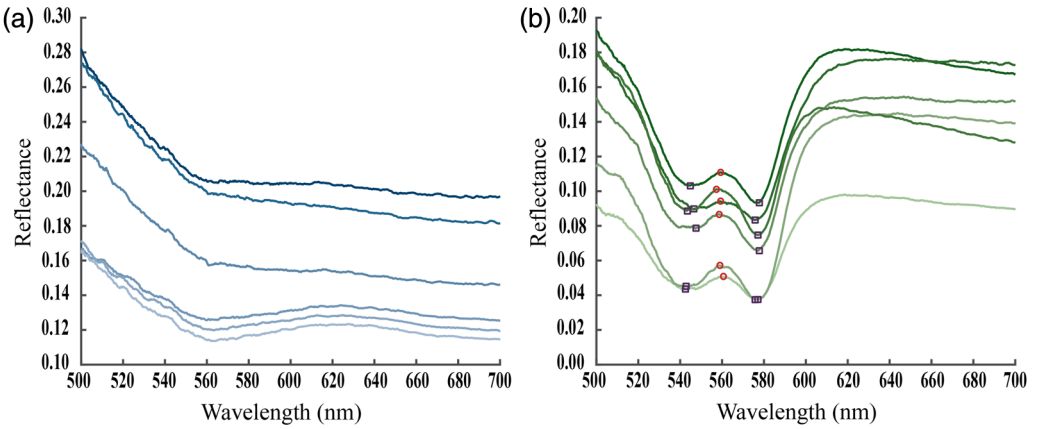

Fig. 8 (a) Smoothed esophageal spectra from pigs 1 and 2. (b) Smoothed tracheal spectra from pigs 1 and 2 with detected minima highlighted by the open boxes and the local maxima circled.

Table 1 Mean wavelength occurrence of minima and maxima of tracheal and esophageal data. For tracheal tissue: point 1 and point 3 correspond to minima, whereas point 2 represents the maximum. For esophageal tissue: point 1 and 3 represent maxima, whereas point 2 represents the minimum.

	Point 1		Point 2		Point 3	
Tissue	Mean λ (nm)	Standard deviation	Mean λ (nm)	Standard deviation	Mean λ (nm)	Standard deviation
Trachea	541.25	4.84	559.89	1.42	576.40	0.83
Esophagus	531.35	1.20	571.00	5.56	578.50	1.80

Using the identified local minima and maxima, we further characterized the respective patterns by quantifying the amplitude, distance, and slope between each point for each individual capture for each tissue. The calculated values were then averaged for each pig and averaged across all pigs to calculate the overall mean amplitude, mean distance, and mean slope, as reported in Table 2. Negative values indicate a decrease in relative reflection.

An independent t-test was also performed on the group of mean amplitudes, distances, and slope values for each pig ($n = 8$) to compare between the two tissue types. For the purpose of comparison, absolute values were used in the

Table 2 Amplitudes, distances, and slopes between minima and maxima for each tissue type. For tracheal tissue: point 1 and point 3 correspond to minima, whereas point 2 represents the maximum. For esophageal tissue: point 1 and 3 represent maxima, whereas point 2 represents the minimum.

	Point 1 to Point 2					
Tissue	Mean amp (E-03)	Standard deviation (E-03)	Mean distance (nm)	Standard deviation (nm)	Mean slope (E-03)	Standard deviation (E-03)
Trachea	8.23	2.63	18.65	6.10	0.48	0.16
Esophagus	−23.00	12.58	39.65	6.18	−0.57	0.24
P-value	0.00879		0.00002		0.41224	
	Point 2 to Point 3					
Tissue	Mean amp (E-03)	Standard deviation (E-03)	Mean distance (nm)	Standard deviation (nm)	Mean slope (E-03)	Standard deviation (E-03)
Trachea	−10.63	6.33	16.50	1.95	−0.60	0.30
Esophagus	2.31	0.93	8.09	5.55	0.55	0.37
P-value	0.00403		0.00201		0.78727	

calculation. As shown in Table 2, there was a significant difference in the amplitudes and distances for the mean amplitude and distances between both pairs of points. On the contrary, the absolute values of the average slopes did not differ significantly for either pairs of points.

4 Discussion

The present studies began for the purpose of exploring the possibility of differences in the spectral responses of tracheal versus esophageal tissues. With the primary motivation stemming from finding a more reliable and readily accessible method of tracheal confirmation during intubations in emergency medicine, we endeavored to explore detection and analysis techniques that could be employed in the prehospital environment.

To first look for and capture any unique spectral properties with high resolution, our study began with *ex vivo* investigations of the tissue responses when exposed to white light using a hyperspectral camera. The *ex vivo* studies exposed a difference in reflectance spectra between the two tissue types, as seen qualitatively in Sec. 3.1 (Fig. 4). In particular, the distinct peak that occurred between 530 and 580 nm in the tracheal reflectance spectrum was dramatically unique from the esophageal reflectance spectrum across the same region, which exhibited a steady decline. Within the tracheal spectra, the most notable characters were the local minima at 541.6 and 577.7 nm with a maximum at 560.9 nm. We believe that the difference in this specific character stems from the physiological differences in the tissue composition, with the trachea primarily consisting of thin connective tissue and cartilage, whereas the esophagus primarily comprises the luminal lining surrounded by thicker, smooth muscle. As we progress in our studies of these spectral characteristics of tracheal and esophageal tissues, especially under variable environments, we plan to continue parallel research into the underlying tissue interaction mechanisms responsible for the observed pattern.

To further compare the relative reflectance strengths for each tissue type at these three notable wavelength bands, single-band images were evaluated at 541.6, 560.9, and 577.7 nm, as depicted in Fig. 5. Despite the noise from the narrow bandwidth and filtering, the 560.9-nm band [Fig. 5(b)] for the tracheal tissue appears significantly brighter than either the 541.6- or 577.7-nm bands [Figs. 5(a) and 5(c)]. On the other hand, the 560.9-nm band of the esophageal tissue [Fig. 5(e)] appears slightly darker with relatively little distinction from that of the 541.6- or 577.7-nm bands [Figs. 5(d) and 5(f)]. The strong distinction in comparison of relative intensities among these three bands provides a potential basis for tissue discrimination using discrete components, such as single-wavelength filters and discrete logic components.

Continuing the investigation with the potential for discrete component implementation in mind, we aimed to explore the detectability of this character of tracheal tissue using more portable technologies and with the tissue in its natural structure, *in situ*. Using a fiber optic sensor *in situ* pig models, we captured and quantified the same unique spectral characteristics of the trachea occurring between the same 530 and 580 nm region-of-interest. Using principal component analysis (PCA), we were able to reiterate the uniqueness of the two different spectral reflectance profiles by grouping all individual captures together, as shown in Fig. 7. Hypothesizing that the first two PCs of the entire dataset would reflect each of the esophageal and tracheal data, the positive correlation coefficients confirm the relationship of the esophageal data with PC1 and the tracheal data with PC2, while the negative correlation coefficients of the inverse pairing show that they are distinctly unique. The approach of employing PCA to extract the PCs of a combined dataset involving multiple tissue types shows its power as a potential technique for tissue classification pertaining to unique spectral reflectance properties.

However, with our primary motivation focusing on utilizing these unique characteristics for future development of an optical device for tracheal detection, we endeavored to distill the characteristics into more simplistic, quantitative differentiations that could be implemented with discrete components or filters. Thus, our investigation into the detection of maxima and minima for both tissues within the previously identified region of interest, 530 to 580 nm, highlighted the consistent pattern of two local minima and one local maximum of the tracheal tissue. Conversely, the spectral profile of esophageal tissue continued to exhibit a pattern of steady decline over the same region. The *in situ* results corroborated the *ex vivo* findings and supported the consistency of the tracheal peak around 560 nm with the data showing 559.89 ± 1.42 nm. In addition, the minimum following the peak in tracheal tissue (second minimum) exhibited equivalent reliability in its occurrence of 576 ± 0.83 nm. While the mean wavelength occurrence of the maximum in the esophagus showed low standard deviations as well, 531.35 ± 1.20 nm and 578.5 ± 1.8 nm, the mean values, themselves, note that these occur at the edges of the region-of-interest. This is further supported by the mean distances calculated for the points on the esophageal spectra. The first interval shows a large average distance, 39.65 nm, followed by a significantly smaller second interval distance of 8.09 nm. Therefore, this result is attributed more to the overall gradual decrease in reflectivity of the esophageal spectrum over the region rather than consistent characteristics that could be exploited for detection purposes.

Alongside the comparison of the wavelength occurrences of the local minima and maxima, further quantitative comparison of amplitude, distance, and slope characteristics yielded additional differences between the two tissue types. While the amplitudes and distances between each pair of detected points resulted in statistically significant differences between the tissues (Table 2), the absolute values of the slopes did not show a statistically significant difference. However, the more practical difference between the two tissue types is the negative slope of the esophageal tissue over the first interval, while the tracheal tissue exhibits a positive slope. Since this difference was apparent through the negative values of the amplitude, we used the absolute values for the independent *t*-test to investigate whether there was an additional statistical significance in the magnitudes. Therefore, despite the lack of statistical significance in slope magnitude between the two tissues, the finding that the tracheal spectra show an increase in reflection intensity within 540 to 560 nm, while the esophageal spectra exhibit a decrease in reflection, holds great significance in a practical sense for detection purposes. This difference, in particular, could be easily implemented using discrete components and filters to look for a significant increase in reflectance between 540 and 560 nm in order to detect the presence of tracheal tissue. Overall, the identification and characterization of these significant differences using fiber optic sensors confirm the hypothesis that there are distinct characteristics of the tracheal tissue versus

esophageal tissue that can be detected using clinically practical technologies.

A major limitation of the study involved the decision to use the same previously captured calibration spectrum as the references for each test. Ideally, the dark and white references would be recalibrated before each testing procedure to account for light source or sensor degradation. However, this decision was made in order to keep the time between time of death and data collection as short as possible so that the tissue properties would reflect as close to *in vivo* as practicable. The consequences became apparent with the pigs collected toward the end, which resulted in noisier spectra and decreased amplitudes and slopes. Given the promising overall results from this *in situ* study, demonstrating strong detection capabilities using fiber optic sensors, future studies will continue exploration with portable technologies *in vivo* and account more for known instrumentation limitations. Additionally, the fiber probe in the present study was a commercial-off-the-shelf device that was not designed for this particular application, the aperture for the light emission, and collection was perpendicular to that of the face of the tissue. We will also endeavor in future studies to explore the potential of angled or beveled probes to collect more reflectance signal from the tracheal and esophageal walls.

5 Conclusion

Through these *ex vivo* and *in situ* studies investigating the spectral properties of tracheal and esophageal tissue, we have identified and characterized a definitive difference in the reflectance spectra when exposed to white light. The defining tracheal characteristic of two local minima and one maximum observed between 530 and 580 nm exhibited consistent and unique properties that could be detected using clinically relevant technologies, such as fiber optic sensors. We conclude that this unique character could be exploited for tracheal detection purposes using discrete components and filters in order to pursue a more reliable, rapid, and readily available method of tracheal confirmation during intubation. Ongoing studies are investigating the detectability *in vivo* and the applicability toward practical tracheal detection devices leveraging the spectral character as a detection mechanism for tracheal confirmation. In this regard specifically, although we are still in the preliminary stages of prototype development, initial results have been promising and encouraging for continued investigations.

Disclosures

No conflicts of interest, financial or otherwise, are declared by the authors.

Acknowledgments

Support of this work by the Army Research Office of the United States Army Research Laboratory, the Defense Advanced Research Project Agency, and the Oak Ridge Institute for Science and Education is acknowledged. The authors have no conflicts of interest to report pertaining to the present study. *Animal statement*: This study has been conducted in compliance with the Animal Welfare Act, the implementing Animal Welfare Regulations, and the principles of the Guide for the Care and User of Laboratory Animals. *DoD disclaimer*: The opinions or assertions contained herein are the private views of the author and are not to be construed as official or as reflecting the views of the Department of the Army or the Department of Defense.

References

1. R. W. Nuemar et al., "2010 American Heart Association Guidelines for cardiopulmonary resuscitation and emergency cardiovascular care science: part 8: adult advanced cardiovascular life support," *Circulation* **122**(Suppl. 3), S729–S767 (2010).
2. M. A. Cobas et al., "Prehospital intubations and mortality: a level 1 trauma center perspective," *Anesth. Analg.* **109**(2), 489–493 (2009).
3. J. C. Sakles et al., "The importance of first pass success when performing orotracheal intubation in the emergency department," *Acad. Emerg. Med.* **20**(1), 71–78 (2013).
4. K. Hasegawa et al., "Association between repeated intubation attempts and adverse events in emergency departments: an analysis of a multicenter prospective observational study," *Ann. Emerg. Med.* **60**(6), 749–754 (2012).
5. S. A. Bernard et al., "Prehospital rapid sequence intubation improves functional outcome for patients with severe traumatic brain injury: a randomized controlled trial," *Ann. Surg.* **252**(6), 959–965 (2010).
6. X. Combes et al., "Prehospital standardization of medical airway management: incidence and risk factors of difficult airway," *Acad. Emerg. Med.* **13**(8), 828–834 (2006).
7. P. Rudraraju and L. A. Eisen, "Analytic review: confirmation of endotracheal tube position: a narrative review," *J. Intensive Care Med.* **24**(5), 283–292 (2009).
8. P. Berlack et al., "Pre-hospital airway management: guidelines from a task force from the Scandinavian Society for Anaesthesiology and Intensive Care Medicine," *Acta Anaesthesiol. Scand.* **52**(7), 897–907 (2008).
9. S. A. Puntervoll et al., "Rapid detection of oesophageal intubation: take care when using colorimetric capnometry," *Acta Anaesthesiol. Scand.* **46**(4), 455–457 (2002).
10. C. D. Deakin et al., "European resuscitation council guidelines for resuscitation 2010," *Resuscitation* **81**(10), 1305–1352 (2010).
11. W. Rabitsch et al., "Evaluation of an end-tidal portable $ETCO_2$ colorimetric breath indicator (COLIBRI)," *Am. J. Emerg. Med.* **22**(1), 4–9 (2004).
12. T. M. Cook et al., "Major complications of airway management in the UK: results of the Fourth National Audit Project of the Royal College of Anaesthetists and the Difficult Airway Society. Part 2: intensive care and emergency departments," *Br. J. Anaesth.* **106**(5), 632–642 (2011).
13. N. M. Deiorio, "Continuous end-tidal carbon dioxide monitoring for confirmation of endotracheal tube placement is neither widely available nor consistently applied by emergency physicians," *Emerg. Med. J.* **22**(7), 490–493 (2005).

Corinne D. Nawn is a biomedical engineering graduate research fellow with the Oak Ridge Institute of Science and Education supporting the US Army Institute of Surgical Research in Fort Sam Houston, Texas. She received her BS in biomedical engineering from Worcester Polytechnic Institute and is currently a doctoral student in a joint biomedical engineering PhD program at the University of Texas at San Antonio and the University of Texas Health Science Center at San Antonio.

Brian E. Souhan earned his PhD in electrical engineering from Columbia University. He is currently an assistant professor in electrical engineering at the United States Military Academy and a research scientist with the Photonics Research Center. His current research is focused primarily on silicon photonics.

Robert Carter III is an adjunct professor of emergency medicine at University of Texas Health Science Center and has served 18 years as a US Army commissioned officer in a variety of clinical, medical research, command, and staff positions. He received his PhD and MPH from the University of North Texas Health Science Center at Fort Worth, Texas.

Caitlin Kneapler earned her PhD in analytical chemistry from the University of Central Florida. She is currently an ORISE fellow with

the US Food and Drug Administration. Her research is focused on nontargeted screening methods for food matrices using HPLC-MS and chemometric approaches.

Nicholas Fell is the deputy PM (army) for the OSD quantum science and engineering program and recently completed a four-year detail as a visiting scientist in the Photonics Research Center of the USMA. He earned his PhD in chemistry from the University of Illinois and specializes in optical spectroscopy. He has been an author or co-author on 11 open literature papers, 2 book chapters, 27 conference proceedings, and over 70 presentations.

Jing Yong Ye is currently an associate professor in the Department of Biomedical Engineering at the University of Texas, San Antonio. He has published 86 refereed articles, 150 conference papers, and holds 12 patents. He serves as a grant reviewer for federal funding agencies (NIH and NSF), state programs and private foundations. He has also cofounded a biotech company and serves on a company's advisory board and as a professional consultant for five companies.